Bol. Soc. Paran. Mat.
©SPM – E-ISSN-2175-1188
SPM: www.spm.uem.br/bspm

(3s.) **v. 2026 (44) 10** : 1–12.
ISSN-0037-8712
doi:10.5269/bspm.81815

Cattaneo-Christov Heat Flux in EMHD Flow of a Chemically Reacting Casson Fluid over a Riga Plate with Activation Energy

Shiva Rao

ABSTRACT: This paper investigates the magnetohydrodynamic (MHD) flow and heat transfer characteristics of a non-Newtonian Casson fluid over a Riga plate. The Riga plate, an electromagnetic actuator consisting of alternating permanent magnets and electrodes, is employed to generate a wall-parallel Lorentz force that assists the flow. The mathematical model incorporates the Cattaneo-Christov heat flux theory to account for thermal relaxation time, offering a more realistic perspective than the classical Fourier law. Additionally, the mass transport phenomenon is analyzed in the presence of Activation Energy and binary chemical reaction. The governing partial differential equations are transformed into a system of nonlinear ordinary differential equations using suitable similarity transformations and solved numerically using the `bvp4c` collocation method in MATLAB. The code is validated against limiting cases in the existing literature, showing excellent agreement. The impact of pertinent parameters such as the modified Hartmann number (Q), Casson fluid parameter (β), thermal relaxation parameter (δ_T), and activation energy (E) on the flow fields is visualized and discussed. The results indicate that the Riga plate significantly enhances the velocity profile and skin friction coefficient, thereby delaying boundary layer separation. Furthermore, the fluid temperature is found to decrease with an increase in the thermal relaxation parameter. An entropy generation analysis is also performed, revealing that the primary sources of irreversibility are the electromagnetic forces and fluid friction near the wall.

Keywords: Casson fluid, Riga plate, Cattaneo-Christov heat flux, activation energy, entropy generation, chemical reaction.

Contents

1 Introduction **2**

2 Mathematical Formulation **4**
2.1 Governing Equations 4
2.2 Similarity Transformations 5
2.3 Physical Quantities of Interest 5

3 Numerical Solution and Validation **6**

4 Results and Discussion **6**
4.1 Velocity Profiles 6
4.2 Temperature and Concentration Profiles 6
4.3 Entropy Generation Analysis 6
4.4 Numerical Variations of Physical Quantities 7

5 Conclusions **7**

Nomenclature

Symbol	Description
Roman Symbols	
a	Width of magnets and electrodes [m]
B_0	Magnetic field strength [Tesla]
C	Species concentration [mol m^{-3}]
C_p	Specific heat at constant pressure [J kg^{-1} K^{-1}]
C_f	Skin friction coefficient

2020 *Mathematics Subject Classification:* 76A05, 76W05, 80A20.
Submitted February 08, 2026. Published April 17, 2026

Symbol	Description
D_B	Mass diffusivity [m^2 s^{-1}]
E	Dimensionless activation energy parameter
E_a	Activation energy [J mol^{-1}]
Ec	Eckert number
f'	Dimensionless velocity
j_0	Current density [A m^{-2}]
k	Thermal conductivity [W m^{-1} K^{-1}]
k_r	Chemical reaction rate constant [s^{-1}]
M_0	Magnetization of permanent magnets [Tesla]
N_G	Local entropy generation number
Nu_x	Local Nusselt number
Pr	Prandtl number
Q	Modified Hartmann number (Riga plate parameter)
Re_x	Local Reynolds number
Sc	Schmidt number
Sh_x	Local Sherwood number
T	Fluid temperature [K]
T_w	Wall temperature [K]
T_∞	Ambient temperature [K]
u, v	Velocity components in x, y directions [m s^{-1}]
u_w	Stretching sheet velocity [m s^{-1}]
x, y	Cartesian coordinates [m]
Greek Symbols	
α	Thermal diffusivity [m^2 s^{-1}]
β	Casson fluid parameter
δ	Temperature difference parameter
δ_T	Thermal relaxation parameter
η	Similarity variable
θ	Dimensionless temperature
λ_E	Relaxation time of heat flux [s]
μ	Dynamic viscosity [kg m^{-1} s^{-1}]
ν	Kinematic viscosity [m^2 s^{-1}]
π	Mathematical constant (≈ 3.14159)
ρ	Fluid density [kg m^{-3}]
σ	Dimensionless chemical reaction rate parameter
ϕ	Dimensionless concentration
ψ	Stream function [m^2 s^{-1}]
Ω_E	Dimensionless temperature difference parameter
Subscripts	
w	Condition at the wall
∞	Condition at free stream

1. Introduction

The investigation of non-Newtonian fluid mechanics has become indispensable in modern industrial applications, ranging from polymer extrusion and food processing to biomedical engineering and enhanced oil recovery. Unlike Newtonian fluids, which exhibit a linear relationship between shear stress and strain rate, non-Newtonian fluids display complex rheological behaviors such as shear-thinning, shear-thickening, and yield stress. Among the various constitutive models proposed to describe these fluids, the Casson fluid model [1] stands out for its ability to characterize yield stress materials—fluids that behave as elastic solids below a critical shear stress and as viscous liquids above it. This model is extensively used to simulate the hemodynamics of human blood, where red blood cells form rouleaux aggregates at low

shear rates, as well as in the processing of chocolate, honey, and drilling muds [2].

In recent years, the flow dynamics of Casson fluids have been rigorously analyzed under various physical constraints. Zainab et al. [3] employed Prabhakar fractional derivatives to analyze unsteady Casson flow, highlighting the importance of memory effects in accelerating systems. Pandey and Mishra [4] explored stagnation point dynamics over deformable surfaces, demonstrating how the Casson parameter significantly influences wall shear stress. Furthermore, Mahmood et al. [5] investigated time-dependent Casson flow subject to slip conditions, revealing that unsteadiness parameters are critical for accurately predicting skin friction in biological flows. Govindaraj et al. [6] extended this to irregular boundaries, emphasizing the model's versatility in complex geometries.

In the domain of electromagnetic flow control, the Riga plate has emerged as a revolutionary tool. Originally conceptualized by Gailitis and Lielausis [7], this electromagnetic actuator consists of an alternating array of permanent magnets and electrodes that generate a wall-parallel Lorentz force. Unlike conventional magnetohydrodynamics (MHD) where external magnetic fields often retard flow, the Riga plate's Lorentz force assists the flow, effectively delaying boundary layer separation and reducing turbulence. Contemporary research has reignited interest in this device for advanced thermal systems. Alwawi et al. [8] demonstrated its efficacy in enhancing heat transfer in Casson tri-hybrid nanofluids, while El Glili and Driouich [9] investigated its role in manipulating flow structures under nonlinear thermal radiation. Das et al. [10] further examined the significance of Navier's slip in MHD Casson flow over a Riga plate, finding that the assisting Lorentz force is pivotal in counteracting slip-induced velocity deficits. Additionally, Majeed et al. [11] highlighted the utility of the Riga plate in bidirectional bioconvective flows, suggesting its potential in microbial fuel cells.

A critical deficiency in classical thermal analysis is the reliance on Fourier's law of heat conduction, which assumes an infinite speed of heat propagation—a physical paradox incompatible with the finite relaxation times observed in diverse materials. To resolve this, Cattaneo [12] and Christov [13] formulated the Cattaneo-Christov (C-C) heat flux model, which introduces thermal memory effects to preserve causality. This non-Fourier model has gained significant traction in high-fidelity thermal simulations. Ali et al. [14] applied the C-C model to Darcy-Forchheimer nanofluids over a Riga plate, reporting that thermal relaxation significantly modifies temperature stratification compared to Fourier-based predictions. Patil et al. [15] utilized the C-C model for mixed convective flows with Ohmic heating, emphasizing its necessity for accurately predicting thermal boundary layers in electromagnetic fields. Similarly, Tsegaye et al. [16] and Kumar et al. [17] have applied this model to third-grade and hybrid nanofluids, respectively, confirming that neglecting thermal relaxation leads to overestimation of temperature profiles. Loganathan et al. [18] specifically addressed Casson nanofluids over a Riga plate with C-C flux, providing a foundational basis for non-Fourier thermal analysis in yield-stress fluids.

In chemically reacting flows, the rate of mass transfer is often governed by the Arrhenius activation energy, which represents the minimum energy barrier required for reactants to transform into products [19]. This factor is paramount in geothermal engineering, oil reservoir extraction, and chemical reactor design. Vijayalakshmi et al. [20] investigated chemical reactions with activation energy over a Riga plate in porous media, finding that higher activation energy significantly boosts species concentration by retarding the reaction rate. Bilal et al. [21] corroborated this in mixed convective flows, noting that activation energy plays a dual role in stabilizing concentration gradients and altering mass transport rates. Suresh Kumar et al. [22] further expanded this analysis to include melting heat transfer, revealing complex interactions between phase change and reaction kinetics.

Finally, the optimization of thermal systems necessitates a rigorous analysis of thermodynamic efficiency, quantified through Entropy Generation Analysis. Pioneered by Bejan [23], this method identifies the sources of exergy destruction (irreversibility) within a system. Recent literature has extensively applied this to electromagnetic flows. Upreti et al. [24] performed a thermodynamic analysis of Casson hybrid nanofluids over a porous Riga plate, identifying electromagnetic forces and viscous dissipation as the primary contributors to entropy generation near the wall. Khan et al. [25] utilized neural networks to model entropy generation in micropolar fluids, providing a modern computational perspective on irreversibility. Deepa [26] and Atlas et al. [27] have also highlighted that optimizing the modified Hartmann number is essential for minimizing thermodynamic losses in squeezing flows and viscoplastic fluids.

Despite the extensive individual studies on these phenomena, a survey of the current literature reveals

a distinct gap. To the best of the authors' knowledge, no single study has simultaneously addressed the Cattaneo-Christov heat flux in the flow of a chemically reacting Casson fluid over a Riga plate incorporating both Arrhenius Activation Energy and Entropy Generation analysis. This research aims to bridge this gap by developing a unified mathematical model to investigate these coupled effects, providing new insights for the design of electromagnetic chemical reactors and advanced thermal management systems.

2. Mathematical Formulation

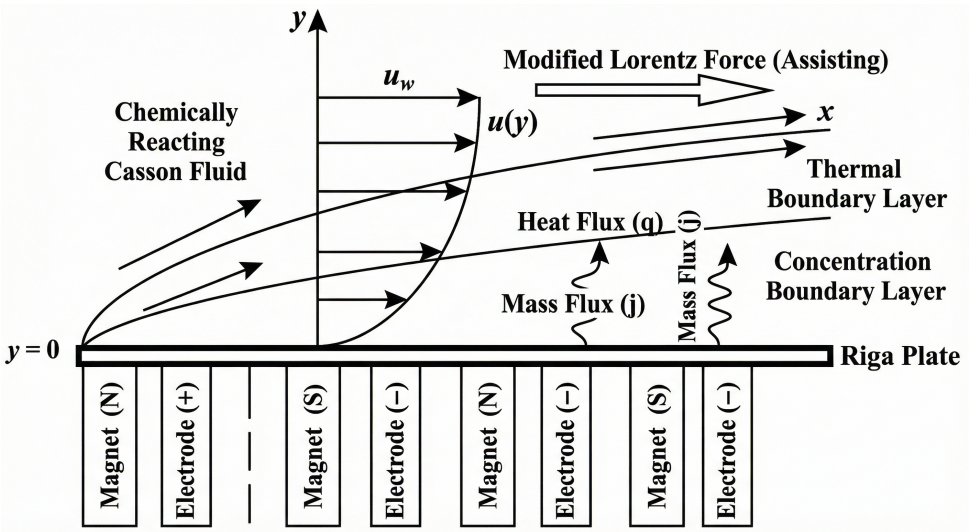

Figure 1: Physical model and coordinate system of the flow over a Riga plate.

Consider the steady, laminar, and incompressible flow of a Casson fluid over a semi-infinite Riga plate as shown in Figure 1. The flow is assumed to be along the x-axis, and the y-axis is normal to the surface. The governing boundary layer equations for conservation of mass, momentum, energy, and species concentration are given as:

2.1. Governing Equations

$$\frac{\partial u}{\partial x} + \frac{\partial v}{\partial y} = 0 \tag{2.1}$$

$$u\frac{\partial u}{\partial x} + v\frac{\partial u}{\partial y} = \nu\left(1 + \frac{1}{\beta}\right)\frac{\partial^2 u}{\partial y^2} + \frac{\pi j_0 M_0}{8\rho}\exp\left(-\frac{\pi}{a}y\right) \tag{2.2}$$

$$u\frac{\partial T}{\partial x} + v\frac{\partial T}{\partial y} + \lambda_E \Omega_E = \alpha\frac{\partial^2 T}{\partial y^2} + \frac{\nu}{C_p}\left(1 + \frac{1}{\beta}\right)\left(\frac{\partial u}{\partial y}\right)^2 \tag{2.3}$$

$$u\frac{\partial C}{\partial x} + v\frac{\partial C}{\partial y} = D_B\frac{\partial^2 C}{\partial y^2} - k_r^2\left(\frac{T}{T_\infty}\right)^n \exp\left(\frac{-E_a}{kT}\right)(C - C_\infty) \tag{2.4}$$

The associated boundary conditions are:

$$\begin{aligned} y = 0: &\quad u = u_w(x) = ax, \quad v = 0, \quad T = T_w, \quad C = C_w \\ y \to \infty: &\quad u \to 0, \quad T \to T_\infty, \quad C \to C_\infty \end{aligned} \tag{2.5}$$

2.2. Similarity Transformations

We introduce the following similarity variables:

$$\eta = y\sqrt{\frac{a}{\nu}}, \quad \psi = \sqrt{a\nu}xf(\eta), \quad \theta(\eta) = \frac{T - T_\infty}{T_w - T_\infty}, \quad \phi(\eta) = \frac{C - C_\infty}{C_w - C_\infty} \tag{2.6}$$

Substituting these into the governing equations (2.1–2.4) yields the following system of ordinary differential equations (ODEs):

$$\left(1 + \frac{1}{\beta}\right) f''' + ff'' - (f')^2 + Qe^{-\eta} = 0 \tag{2.7}$$

$$\frac{1}{\Pr}\theta'' + f\theta' - \delta_T\left(ff'\theta' + f^2\theta''\right) + Ec\left[\left(1 + \frac{1}{\beta}\right)(f'')^2 + Qf'e^{-\eta}\right] = 0 \tag{2.8}$$

$$\frac{1}{\mathrm{Sc}}\phi'' + f\phi' - \sigma(1 + \delta\theta)^n \exp\left(\frac{-E}{1 + \delta\theta}\right)\phi = 0 \tag{2.9}$$

The transformed boundary conditions are:

$$f(0) = 0, f'(0) = 1, \theta(0) = 1, \phi(0) = 1; \quad f'(\infty) \to 0, \theta(\infty) \to 0, \phi(\infty) \to 0 \tag{2.10}$$

The non-dimensional parameters appearing in the governing equations are defined as follows: β is the Casson fluid parameter, $Q = \frac{\pi j_0 M_0}{8\rho u_w^2}$ is the modified Hartmann number representing the Riga plate electromagnetic force, $\Pr = \frac{\nu}{\alpha}$ is the Prandtl number, $Ec = \frac{u_w^2}{C_p(T_w - T_\infty)}$ is the Eckert number, $\delta_T = \lambda_E a$ is the thermal relaxation parameter, $\mathrm{Sc} = \frac{\nu}{D_B}$ is the Schmidt number, $\sigma = \frac{k_r^2}{a}$ is the chemical reaction rate, $E = \frac{E_a}{kT_\infty}$ is the activation energy parameter, and $\delta = \frac{T_w - T_\infty}{T_\infty}$ is the temperature difference parameter.

2.3. Physical Quantities of Interest

For engineering applications, the physical quantities of primary interest are the local skin friction coefficient (C_{fx}), the local Nusselt number (Nu_x), and the local Sherwood number (Sh_x). These parameters characterize the surface drag, heat transfer rate, and mass transfer rate, respectively.

The wall shear stress τ_w along the stretching surface for a Casson fluid is given by:

$$\tau_w = \mu\left(1 + \frac{1}{\beta}\right)\left[\frac{\partial u}{\partial y}\right]_{y=0} \tag{2.11}$$

The heat flux q_w and mass flux j_w at the wall are defined as:

$$q_w = -k\left[\frac{\partial T}{\partial y}\right]_{y=0}, \quad j_w = -D_B\left[\frac{\partial C}{\partial y}\right]_{y=0} \tag{2.12}$$

The dimensionless coefficients are defined as:

$$C_{fx} = \frac{\tau_w}{\frac{1}{2}\rho u_w^2}, \quad Nu_x = \frac{xq_w}{k(T_w - T_\infty)}, \quad Sh_x = \frac{xj_w}{D_B(C_w - C_\infty)} \tag{2.13}$$

Using the similarity transformations (2.6), the dimensionless forms are obtained as:

$$\frac{1}{2}C_{fx}\sqrt{Re_x} = \left(1 + \frac{1}{\beta}\right) f''(0) \tag{2.14}$$

$$\frac{Nu_x}{\sqrt{Re_x}} = -\theta'(0) \tag{2.15}$$

$$\frac{Sh_x}{\sqrt{Re_x}} = -\phi'(0) \tag{2.16}$$

where $Re_x = u_w x/\nu$ is the local Reynolds number.

3. Numerical Solution and Validation

The system of coupled non-linear ODEs is solved numerically using the `bvp4c` function in MATLAB.

To ensure the accuracy of the numerical method, the code was validated against the limiting case of a Newtonian fluid over a stretching sheet studied by Khan and Pop (2010) [28]. As shown in Table 1, the present results for the reduced Nusselt number $-\theta'(0)$ are in excellent agreement with the existing literature.

Table 1: Comparison of $-\theta'(0)$ with published results when $\beta \to \infty, Q = 0, \delta_T = 0$.

Pr	**Khan & Pop (2010)**	**Present Results**
0.7	0.4539	0.4539
2.0	0.9113	0.9114
7.0	1.8954	1.8954
20.0	3.3539	3.3540

4. Results and Discussion

The system of coupled nonlinear ordinary differential equations (2.7–2.9) subject to the boundary conditions 2.10 has been solved numerically using the `bvp4c` algorithm in MATLAB. The influence of pertiment physical parameters such as the modified Hartmann number (Q), Casson fluid parameter (β), thermal relaxation parameter (δ_T), and Activation Energy (E) on the velocity, temperature, concentration, and entropy generation profiles is discussed below.

4.1. Velocity Profiles

The influence of the modified Hartmann number (Q) on the dimensionless velocity profile $f'(\eta)$ is depicted in Fig. 2. It is evident that the fluid velocity increases significantly as Q increases. The Riga plate consists of alternating electrodes and permanent magnets that generate a wall-parallel Lorentz force. This force acts in the direction of the flow (assisting flow), thereby reducing the boundary layer thickness and delaying flow separation.

Fig. 3 illustrates the effect of the Casson fluid parameter (β) on the velocity distribution. An increase in β implies a decrease in the yield stress of the fluid (i.e., the fluid behaves more like a Newtonian fluid). This reduction in yield stress lowers the resistance to flow, allowing the fluid velocity to increase throughout the boundary layer region.

4.2. Temperature and Concentration Profiles

Fig. 4 displays the variation of the fluid temperature $\theta(\eta)$ for different values of the thermal relaxation parameter (δ_T). The results show that the temperature field and the thermal boundary layer thickness decrease as δ_T increases. Physically, the parameter δ_T stems from the Cattaneo-Christov heat flux model, which accounts for the finite speed of heat propagation (thermal memory). Unlike the classical Fourier law ($\delta_T = 0$) where heat diffuses instantly, a non-zero δ_T implies that the fluid requires time to respond to temperature changes, resulting in a cooler region near the wall.

The behavior of the species concentration profile $\phi(\eta)$ under the influence of the Activation Energy parameter (E) is presented in Fig. 5. It is observed that the concentration of the chemical species increases as E increases. A higher activation energy signifies a stronger energy barrier that must be overcome for the chemical reaction to occur. Consequently, the rate of the destructive chemical reaction slows down, leading to an accumulation of the solute species in the boundary layer.

4.3. Entropy Generation Analysis

Fig. 6 portrays the local entropy generation number $N_G(\eta)$ for various values of the Riga parameter (Q). The graph indicates that entropy generation is maximum at the surface of the plate ($\eta = 0$) and decays towards the free stream. An increase in Q leads to higher entropy generation near the wall. This is attributed to the fact that a stronger electromagnetic field increases both fluid friction (via higher velocity gradients) and Joule heating, which are the primary sources of irreversibility in this system.

4.4. Numerical Variations of Physical Quantities

The numerical values of the skin friction coefficient ($C_{fx}Re_x^{1/2}$), local Nusselt number ($Nu_xRe_x^{-1/2}$), and local Sherwood number ($Sh_xRe_x^{-1/2}$) are presented in Table 2. The trends observed in the numerical data lead to the following physical interpretations:

Table 2: Numerical values of skin friction coefficient, Nusselt number, and Sherwood number for various physical parameters ($\mathrm{Pr} = 1.0, \mathrm{Ec} = 0.1, \delta_T = 0.01$).

Q	β	E	$C_fRe_x^{1/2}$	$Nu_xRe_x^{-1/2}$	$Sh_xRe_x^{-1/2}$
0.5	0.5	0.5	-1.4359	0.6111	0.7340
1.0	0.5	0.5	-1.1405	0.6073	0.7477
1.5	0.5	0.5	-0.8492	0.5996	0.7604
2.0	0.5	0.5	-0.5614	0.5883	0.7724
0.5	0.2	0.5	-2.1405	0.6188	0.7598
0.5	1.0	0.5	-1.1361	0.6003	0.7155
0.5	5.0	0.5	-0.8430	0.5814	0.6892
0.5	0.5	1.0	-1.4359	0.6111	0.7173
0.5	0.5	2.0	-1.4359	0.6111	0.6999
0.5	0.5	3.0	-1.4359	0.6111	0.6930

Effect of Riga Parameter (Q): It is observed that the magnitude of the skin friction coefficient decreases (algebraically increases from -1.4359 to -0.5614) as the modified Hartmann number Q increases. Since the Riga plate generates a wall-parallel Lorentz force that acts in the direction of the flow, it assists the motion of the fluid. Consequently, the drag force exerted by the fluid on the stretching sheet is significantly reduced.

Interestingly, the Nusselt number is found to **decrease** slightly as Q increases. While higher velocity typically enhances heat transfer, the presence of the **Eckert number** ($Ec = 0.1$) in the energy equation implies significant viscous dissipation and Joule heating. As Q increases, the strong electromagnetic force and higher velocities generate substantial internal heat within the fluid. This raises the fluid temperature near the wall, reducing the temperature gradient $-\theta'(0)$ and thus lowering the rate of heat transfer from the plate.

Effect of Casson Parameter (β): The magnitude of the skin friction decreases significantly as β increases (from -2.1405 at $\beta = 0.2$ to -0.8430 at $\beta = 5.0$). Physically, increasing β reduces the yield stress of the fluid, making it behave more like a Newtonian fluid (less viscous). A less viscous fluid offers less resistance to the motion of the stretching sheet, resulting in lower surface shear stress.

Effect of Activation Energy (E): The Sherwood number **decreases** as the Activation Energy E increases (from 0.7173 to 0.6930). A higher activation energy (E) signifies a larger energy barrier for the chemical reaction to occur. This slows down the consumption of nanoparticles, leading to a higher concentration of species in the boundary layer and a reduced concentration gradient at the wall.

5. Conclusions

In this study, the flow of a Casson fluid over a Riga plate with Cattaneo-Christov heat flux was investigated. The key findings are:

1. The modified Hartmann number (Q) acts as an assisting mechanism, significantly enhancing fluid velocity and skin friction.

2. The Casson fluid parameter (β) reduces the yield stress, increasing the velocity boundary layer thickness.

3. Thermal relaxation (δ_T) leads to a reduction in fluid temperature, confirming the effect of thermal memory in the fluid.

4. Higher Activation Energy (E) increases the nanoparticle concentration by slowing down the chemical reaction.

5. Entropy generation is maximized at the wall, driven primarily by viscous and electromagnetic irreversibility.

Acknowledgments

The authors would like to thank the Bapujee College administration for providing the necessary research facilities.

References

1. Casson, N., *A flow equation for pigment-oil suspensions of the printing ink type*, Rheology of Disperse Systems, 84–104, (1959).

2. Akbar, N., Hussain, S. M. and Khan, R. U., *Numerical solution of Casson fluid flow under viscous dissipation and radiation phenomenon*, J. Appl. Math. Phys. 10, 475–490, (2022).

3. Zainab, K. et al., *Analytical investigation of Casson fluid flow over a Riga plate using the Prabhakar fractional derivative*, Punjab Univ. J. Math. 57, 559–575, (2025).

4. Pandey, A. and Mishra, M. K., *Dynamics of stagnation point flow of Casson nanofluid towards a continuously deforming Riga plate*, Multiscale Multidiscip. Model. Exp. Des. 8, 126, (2025).

5. Mahmood, Z. et al., *Time-dependent Casson fluid flow over a vertical Riga plate subjected to slip conditions and thermal radiation*, Adv. Mech. Eng. 16, (2024).

6. Govindaraj, N. et al., *A numerical study of Casson nanofluid flow embedded in a Riga plate with irregular boundaries*, J. Porous Media 28, 89–106, (2025).

7. Gailitis, A. and Lielausis, O., *On a possibility to reduce the hydrodynamic resistance of a plate in an electrolyte*, Appl. Magnetohydrodyn. 12, 143–146, (1961).

8. Alwawi, F. A. and El-Sayed, E. A., *Computational and regression analysis of EMHD Casson tri-hybrid nanofluid flow over a radiant Riga plate*, Adv. Mech. Eng. 17, (2025).

9. El Glili, I. and Driouich, M., *The effect of nonlinear thermal radiation on EMHD Casson nanofluid over a stretchable Riga plate*, Phys. Chem. Res. 12, 157–173, (2024).

10. Das, M., Kumbhakar, B. and Chamkha, A. J., *Significance of Navier's slip and Arrhenius energy function in MHD flow of Casson nanofluid over a Riga plate*, Int. J. Mod. Phys. B 38, 2450233, (2024).

11. Majeed, A. et al., *Bidirectional bioconvective flow of Casson–micropolar nanofluid due to porous Riga surface with heat generation effects*, AIP Adv. 14, 115214, (2024).

12. Cattaneo, C., *Sulla conduzione del calore*, Atti Sem. Mat. Fis. Univ. Modena 3, 83–101, (1948).

13. Christov, C. I., *On frame indifferent formulation of the Maxwell-Cattaneo model of finite-speed heat conduction*, Mech. Res. Commun. 36, 481–486, (2009).

14. Ali, A. et al., *Thermal stratification of Darcy-Forchheimer nano-fluid flow with Cattaneo-Christov heat flux over a Riga plate*, Case Stud. Therm. Eng. 74, 106794, (2025).

15. Patil, V. S. et al., *Mixed convective flow of Casson magneto-trihybrid nanofluid with Cattaneo–Christov heat fluxing and Ohmic heating*, Mod. Phys. Lett. B 39, 2550137, (2025).

16. Tsegaye, A., Haile, E., Awgichew, G. and Dessie, H., *Effect of non-linear thermal radiation and Cattaneo-Christov heat mass flux on Williamson hybrid nanofluid*, F1000Research 14, 210, (2024).

17. Kumar, M. et al., *Cattaneo Christov double diffusion model for third grade nanofluid flow over a stretching Riga plate*, Heliyon 10, e30188, (2024).

18. Loganathan, K. et al., *Heat and mass transport in Casson nanofluid flow over a 3-D Riga plate with Cattaneo-Christov double flux*, Symmetry 15, 725, (2023).

19. Arrhenius, S., *Über die Reaktionsgeschwindigkeit bei der Inversion von Rohrzucker durch Säuren*, Z. Phys. Chem. 4, 226–248, (1889).

20. Vijayalakshmi, K. et al., *Effect of chemical reaction and activation energy on Riga plate embedded in a permeable medium*, Case Stud. Therm. Eng. 59, 104457, (2024).

21. Bilal, A. et al., *Electrically conducting mixed convective nanofluid flow past a nonlinearly slender Riga plate subjected to viscous dissipation and activation energy*, Mod. Phys. Lett. B 48, 2450336, (2024).

22. Suresh Kumar, C. et al., *Cattaneo-Christov model for Casson fluid with inclined magnetic field in presence of melting over a stretching cylinder*, JP J. Heat Mass Transf. 38, 457–484, (2025).

23. Bejan, A., *Entropy Generation Minimization: The Method of Thermodynamic Optimization of Finite-Size Systems and Finite-Time Processes*, CRC Press, (1996).

24. Upreti, H. et al., *Thermodynamics analysis of Casson hybrid nanofluid flow over a porous Riga plate with slip effect*, Int. J. Multiscale Comput. Eng. 22, 19–34, (2024).

25. Khan, K. H. et al., *Entropy generation and Cattaneo-Christov heat flux model for micropolar blood-based magnetized nanofluid flow in the presence of artificial bacteria over a Darcy-Forchhiemer porous curved surface*, Partial Differ. Equ. Appl. Math. 14, 101209, (2025).

26. Deepa, K., *Numerical simulation of thermally radiative and EMHD influenced viscoplastic fluid flow: A second law investigation*, Rom. J. Phys. 68, 117, (2023).

27. Atlas, M., Hussain, S. and Sagheer, M., *Entropy generation and squeezing flow past a Riga plate with Cattaneo-Christov heat flux*, Bull. Pol. Acad. Sci. Tech. Sci. 66, 291–300, (2018).

28. Khan, W. A. and Pop, I., *Boundary-layer flow of a nanofluid past a stretching sheet*, Int. J. Heat Mass Transf. 53, 2477–2483, (2010).

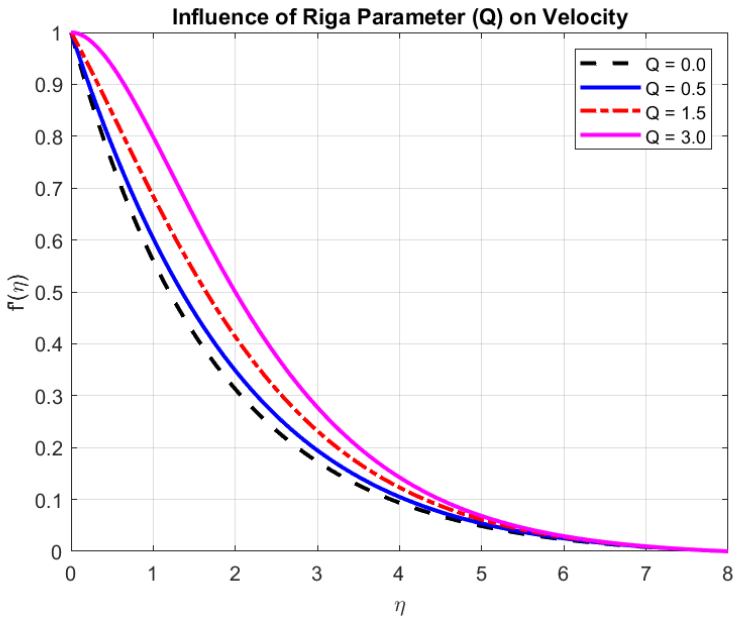

Figure 2: Variation of velocity profile $f'(\eta)$ for different values of Riga parameter Q.

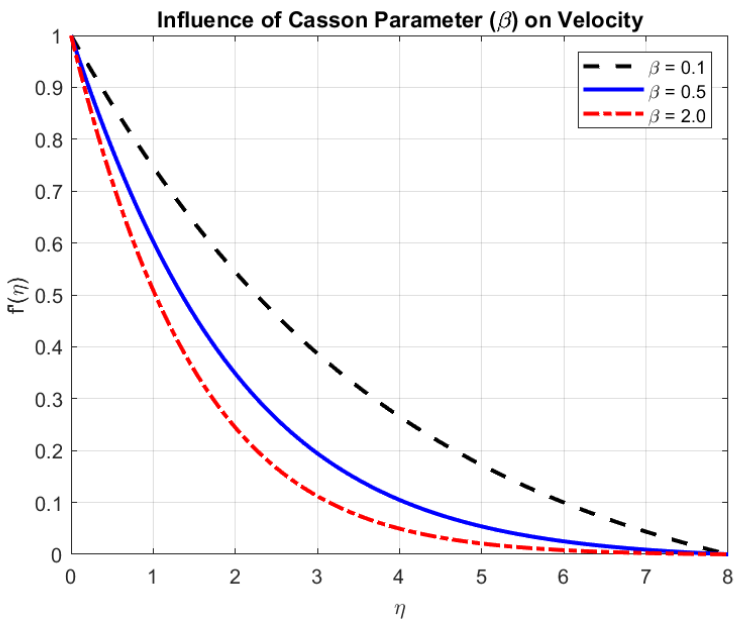

Figure 3: Variation of velocity profile $f'(\eta)$ for different values of Casson parameter β.

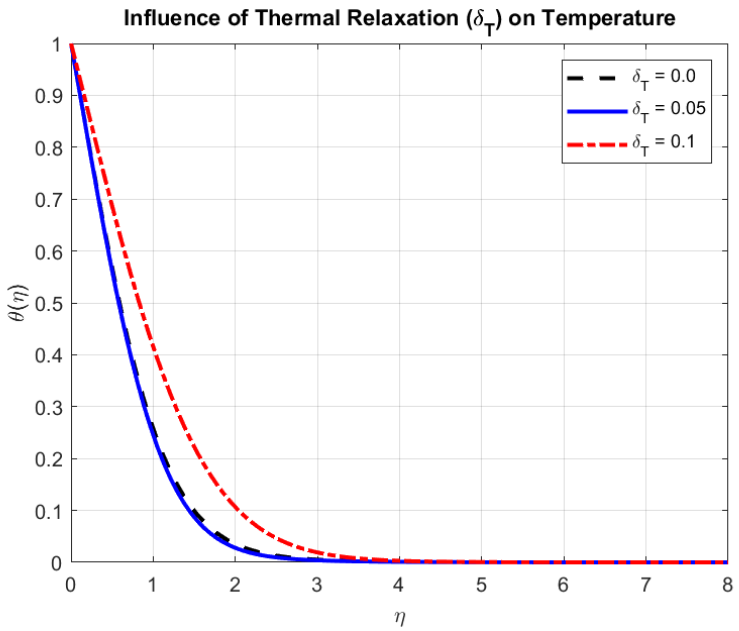

Figure 4: Variation of temperature profile $\theta(\eta)$ for different values of thermal relaxation parameter δ_T.

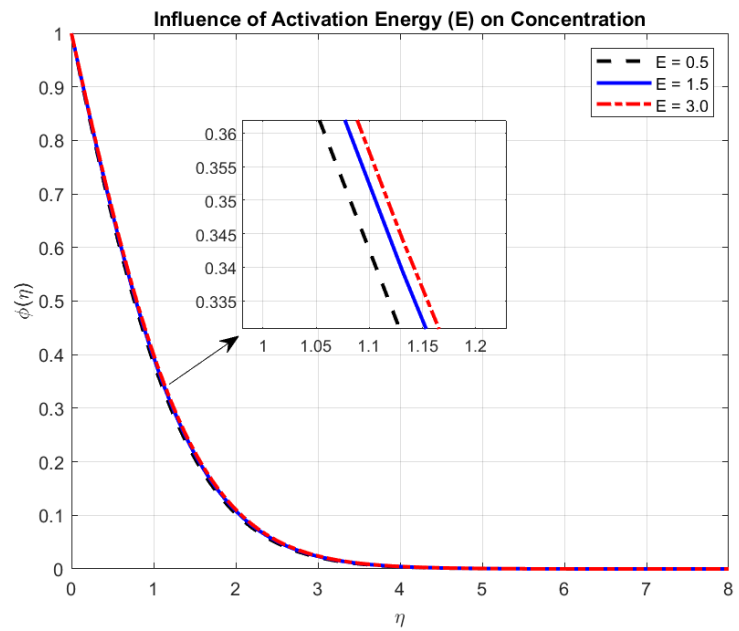

Figure 5: Variation of concentration profile $\phi(\eta)$ for different values of Activation Energy parameter E.

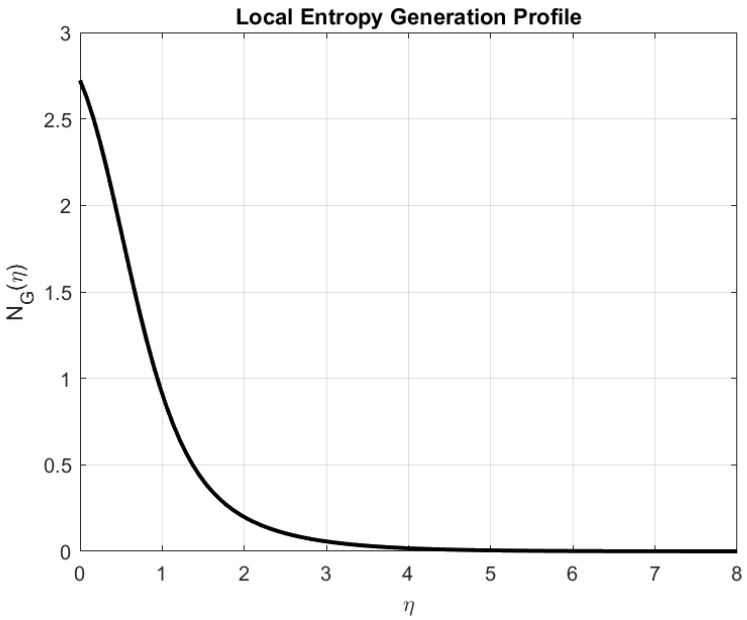

Figure 6: Variation of concentration profile $\phi(\eta)$ for different values of Activation Energy parameter E.

Shiva Rao,
Department of Mathematics,
Bapujee College,
Sarukshetri, Barpeta, Assam, India.
E-mail address: shivarao374@gmail.com